Scientific Research Publishing

International Journal of Geosciences, 2024, 15, 698-719
https://www.scirp.org/journal/ijg
ISSN Online: 2156-8367
ISSN Print: 2156-8359

# The Dynamic Impact of Ocean on Continent

**Yongfeng Yang**

Water Resources Comprehensive Development Center, Bureau of Water Resources of Shandong Province, Jinan, China
Email: roufeng_yang@outlook.com

**How to cite this paper:** Yang, Y.F. (2024) The Dynamic Impact of Ocean on Continent. *International Journal of Geosciences*, **15**, 698-719.
https://doi.org/10.4236/ijg.2024.159039

**Received:** September 2, 2024
**Accepted:** September 21, 2024
**Published:** September 24, 2024



## Abstract

Around 71% of the Earth's surface is covered by oceans with depths that exceed several kilometers, while continents are geographically enclosed by these vast bodies of water. The principle of fluid mechanics stipulates that water yields pressure everywhere in the container that holds it, and the water pressure against the wall of container generates force. Ocean basins are naturally gigantic containers of water, in which continents form the walls of the containers. In this study, we present that the ocean water pressure against the walls of continents generates enormous force, and determine the distribution of this force around continents and estimate its amplitude to be of the order of $10^{17}$ N per kilometer of continent width. Our modelling suggests that the stresses yielded by this force are mostly concentrated on the upper part of the continental crust, and their magnitudes reach up to 2.0 - 6.0 MPa. Our results suggest that the force may have significantly impacted the dynamics of continent (lithospheric plate) and its evolution.

## Keywords

Ocean, Water Pressure Force, Continent, Ocean-Continent Interaction, Stress, Earthquake, Plate Motion

## 1. Introduction

The co-existence of ocean and continent makes the Earth unique in the solar system. Covering roughly 71% of the planet's surface, oceans hold a volume of almost 1.35 billion km$^3$, with an average depth of nearly 3700 meters [1]. Contrastingly, continents occupy around 29% of Earth's surface and are geographically enclosed by these vast bodies of water. Mechanically, if a liquid and a solid are put together, they must interact with each other. The present study of ocean-continent interaction is focused mostly on the transition zone, where sea water erodes coast while land contributes sediment to seafloor, and the exchange of material, energy, and information takes place extensively [2] [3]. The principle of fluid mechanics

stipulates that water pressure against the wall of a container that holds the water generates force. Ocean basins are naturally gigantic containers of water, in which continents form the walls of these containers. Hence, the ocean water pressure against the wall of continent may generate enormous force. Even so, the details of this force, including its magnitude and direction, are still unclear. Geochemical research on zircons indicates that the existence of liquid water on Earth is more than 4 billion years [4]-[6]. During such a long geological timescale, ocean water pressure force may exert impact on continents, since continents would deform in response to any external force. Moreover, continents are physically fixed at the top of the lithospheric plates, this attachment allows the force to be laterally transferred to the lithospheric plates. From these points, addressing the ocean water pressure force is very important for understanding the dynamics of continent (lithospheric plate) and its evolution. The objects of this study are twofold, first, to present a new force generated by ocean water; secondly, to explore the stress caused by this force in the continent and its implication.

## 2. Force between Water and Rocky Material

In recent years, I have met a view stating that the difference in lateral density causes continent to extend over ocean. They think that, since the continent's density is greater than the ocean's density, the lateral density difference yields a force that drives continent to extend over ocean. The issue raised by this view is vital because it relates to the principle of fluid mechanics, and hence deserves a wider discussion. First of all, the view contradicts the basic knowledge of fluid mechanics. As illustrated in **Figure 1(a)**, we compare the hydrostatic pressure within a water body with the lithostatic pressure within a rock body. Given the two points, p1 and p2, are situated at the same depth of the water body and the rock body, respectively, the lithostatic pressure must be higher due to the rock's greater density. Water pressure differs from rock pressure in that the former arises from the weight and movement of water molecules, whereas the latter arises solely from the weight of rocky materials. The rocky materials within continent are highly viscous and self-constrained, making it difficult for them to flow freely. Conversely, a low viscosity of water allows water particles to flow freely. This difference in physics property explains why a rock body can maintain its shape, while a water body conforms to the container holding it. Next, as illustrated in **Figure 1(b)**, we put the water body and the rock body together. Since the water body performs more mobile than the rock body does, some of the water body tends to flow towards the rock body and therefore exerts pressure force on the rock body. Further, as illustrated in **Figure 1(c)**, we put water into a container composed of rocky materials, the water exerts pressure force on the walls of the container. Second, I have asked experts regarding the question of whether or not ocean pushes continent. Several feedbacks support my argument above. There is a comment from Dr. John M. Cimbala: "*Think about an empty tea cup sitting in a vacuum chamber with zero pressure. There is certainly internal pressure in the walls of the tea cup. However*,

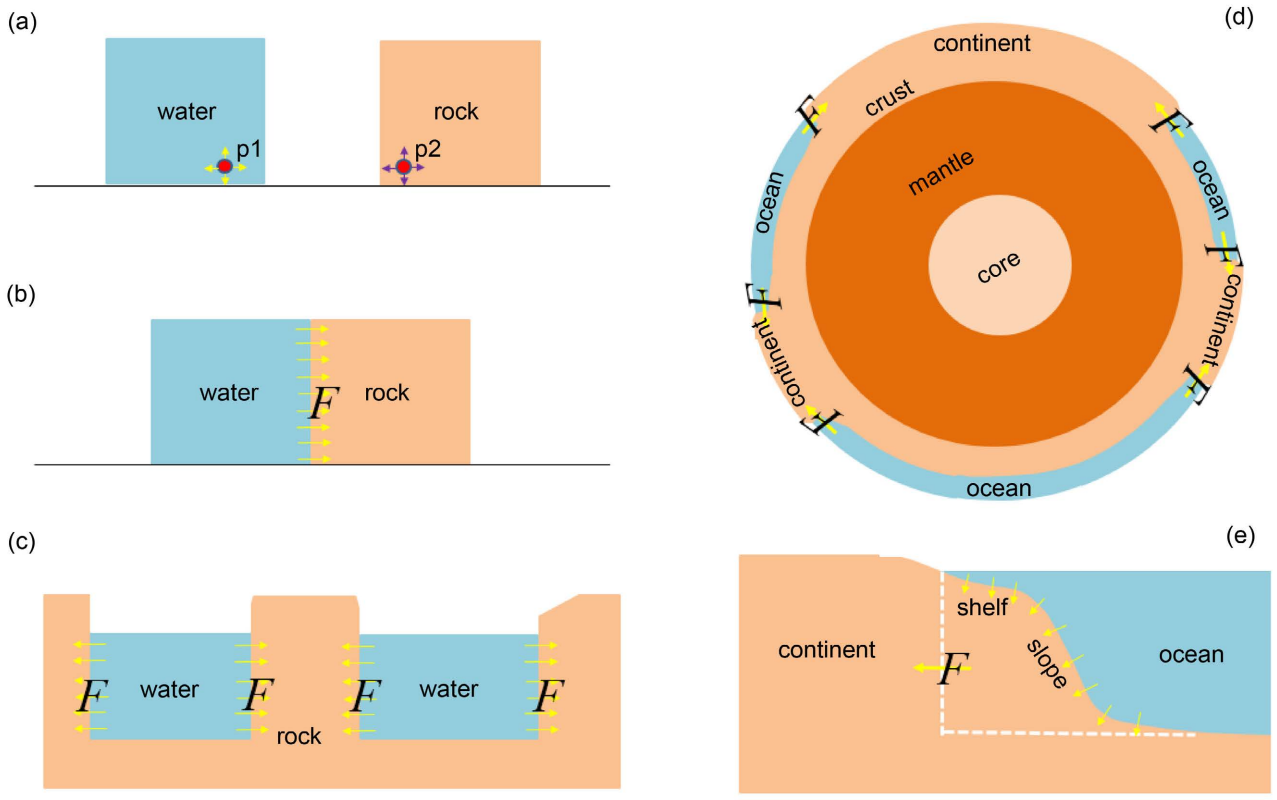


**Figure 1.** Conceptual model of the force between water and rock. (a) Pressure comparison between water body and rock body. (b) A lateral pressure force appears when the two bodies are put together. (c) Water pressure force exerted on the container's walls. (d) Ocean water pressure force exerted on the walls of continents. (e) Water pressure force geometry between ocean and continent. *F* represents the water pressure force.

*those walls do not exert any kind of pressure or force on the surroundings* (*which is a vacuum*). *And the cup stays the same shape and holds its shape regardless of its surroundings. Now take the cup out of the vacuum chamber and into the air. Now air exerts a pressure on the cup walls. The cup walls exert and equal and opposite pressure on the air due to Newton's third law. Now fill the cup with water. The pressure inside the cup increases, and the cup expands ever so slightly, but it still maintains its shape. The cup exerts pressure on the water and vice-versa. But it is the water that causes this pressure, not the cup. Water is a liquid and cannot maintain its shape unless it is in some kind of container. That is where the pressure comes from.*" As illustrated in **Figure 1(d)**, the continents are staying in the uppermost part of the Earth's crust. The formation of the Earth's crust was earlier than the appearance of liquid water, because the crust provides place for liquid water to be hold. The loading of liquid water onto the Earth's crust is just like that water is filled into the tea cup. Therefore, when ocean basins are treated as containers, the ocean water must exert pressure force on the walls of the continents. There is another comment from Dr. Chris Hughes: "*The ocean does indeed push on the continents, and they push back with an equal pressure. The force that makes things move is the gradient of the stress tensor, which in the ocean is effectively the pressure gradient, but in the continents is a combination of pressure and*

*response to internal strains. Without those extra forces, the continents would simply be another, denser fluid, and would flow beneath the ocean.*" There is third comment from Dr. Gerald Shubert: "*If you imagine the edge of a continent to be a vertical plane then the water pressure will push against the continent. But the situation is more complex than that. There are continental shelves that extend under the oceans.*" As illustrated in **Figure 1(e)**, the edge of a continent includes the continental shelf and slope, and they all are situated under the water. If we project them horizontally, a vertical plane can be reached. The ocean water pressure forces exerted on the continental shelf and slope can be geometrically decomposed into horizontal and vertical forces. As a result, all horizontal forces are laterally exerted on that vertical plane. Last, discussing the topic of force has to involve two objects: the object exerting force and the object receiving the force. For one object using force to push another object, the first object has to move (*i.e.*, change its position) to exert force on the second object. As ocean water moves more easily relative to continent, there can be push force from ocean to continent.

## 3. Ocean-Generated Force

As shown in **Figure 2(top)**, according to the principle of fluid mechanics [7], the water pressure force generated on the wall of a cubic container can be expressed as $F = PS = \rho g y^2 x/2$, where $P$ and $S$ are the pressure and wall area, $g$ and $\rho$ are the gravitational acceleration and water density, respectively, and $x$ and $y$ are the water width and depth, respectively, in the container. Ocean basins are naturally gigantic containers, and their depths reach more than a few kilometers and vary from one place to another. Consequently, the application of ocean water pressure against the continent's walls, which are also the sides of ocean basins, can yield enormous forces on continents. Geometrically, as shown in **Figure 2(middle)**, ocean water pressure is exerted vertically to the continental slope, by which a normal force is formed. This normal force is called the ocean-generated force, denoted as $F_R$ on the right and $F_L$ on the left. The horizontal force decomposed from this normal force is denoted as $F_R'\left(F_L'\right)$ on the right (left), while the vertical force decomposed from this normal force is denoted as $F_R''\left(F_L''\right)$ on the right (left). In general, the horizontal force on the wall of continent can be approximately written as

$$F = 0.5\rho g L h^2 \tag{1}$$

where $\rho$, $g$, $L$, and $h$ are the water density, gravitational acceleration, ocean width that fits the continent wall's width, and ocean depth, respectively. And $Lh$ denotes the area of the continent wall.

Practically, continent appears more like a broad cylinder standing in the ocean, and its wall is not flat. We imaginarily project a continent into a polygonal column along the horizontal direction, then dissect the whole wall of this column into smaller rectangular walls connecting one to another, and finally calculate the horizontal force generated on each of these rectangular walls (**Figure 2(middle)**). We now design many geographical sites (e.g. 1, 2, 3, 4, etc.) along the edges of

continents. The latitudes and longitudes of these sites are extracted from the ETOPO1 Global Relief Model (Figure 2(bottom)). A geographical distance between two adjacent sites is calculated using their respective latitudes and longitudes through a spherical geometry, and treated as the width of a smaller rectangular wall. The geographical distance of two sites is expressed as

$$L = R * \arccos\left(\sin\left(q_j\right) * \sin\left(q_{j+1}\right) + \cos\left(q_j\right) * \cos\left(q_{j+1}\right) * \cos\left(d_{j+1} - d_j\right)\right) \quad (2)$$

where $R$ is the Earth's radius and $R = 6371$ km, $q_j$ and $d_j$ are the latitude and longitude of a site, while $q_{j+1}$ and $d_{j+1}$ are the latitude and longitude of another site. Using the NOAA bathymetric data viewer, we estimate the corresponding ocean depth of each rectangular wall. $\rho = 1000$ kg/m$^3$, and $g = 9.8$ m/s. We then use the expression above and these parameters to work out the horizontal forces around continents. It is assumed that the horizontal force exerts on a hypothetical geometric center of the wall, with the direction of the force being orthogonal to the direction of the wall. We use the direction of a side that connects two sites to represent the direction of the wall. Using this direction, the inclination of the force to latitude is determined. The latitude and longitude of the geometric center are established as the average of the latitudes and longitudes of two adjacent sites. The horizontal forces and the parameters for calculating them have been listed in Table 1.

## 4. The Resultant Stress from Ocean-Generated Force

As exhibited in Figure 2, the ocean-generated forces uniformly exert inwards the continents. The continents are situated on the top of continental plates, and therefore, the forces exerted on the plates have inevitably related to the stress in the continents. Our understanding of the stress yielded by ocean-generated force begins with a dynamic distribution around a straight continental plate (Figure 3(a)). We assume that Plate A moves towards the left, Plate B exerts a collisional force ($F_c$) on its left side, the oceanic ridge exerts a push force ($F_{RF}$) on its right side, and the asthenosphere exerts a friction force ($F_b$) on its base, and ocean water exerts pressure forces ($F_{LW}$ and $F_{RW}$) at the two sides of its top. Ridge push force is widely considered either as a boundary force or a body force. As a boundary force, it is derived from a "gravity wedging" effect of a warm, buoyant mantle upwelling and acts at the edge of the lithospheric plate. Turcotte and Schubert [9] outlined the ridge push force through Figure 3(a) and expressed it as $F_{RP} = F_1$-$F_2$-$F_3$, where $F_1 = F_5$, $F_2 = F_4$. Since $F_3$, $F_4$, and $F_5$ relate to the pressure that linearly increases with depth, it may be expected that the minimal ridge push force appears at the uppermost part of the oceanic ridge, whereas the maximal ridge push force appears at the lowermost part. Ocean tides represent the daily regular alternations of high and low water in the oceans. The tides cause the water depth to vary, and thereby, the ocean water pressure varies timely. In consideration of this present status, we demonstrate the resultant stress by means of three combinations of different forces. In reality, the Earth's surface is curved, and the vertical dimension of a continental plate is far less than its horizontal dimension, making it challenging

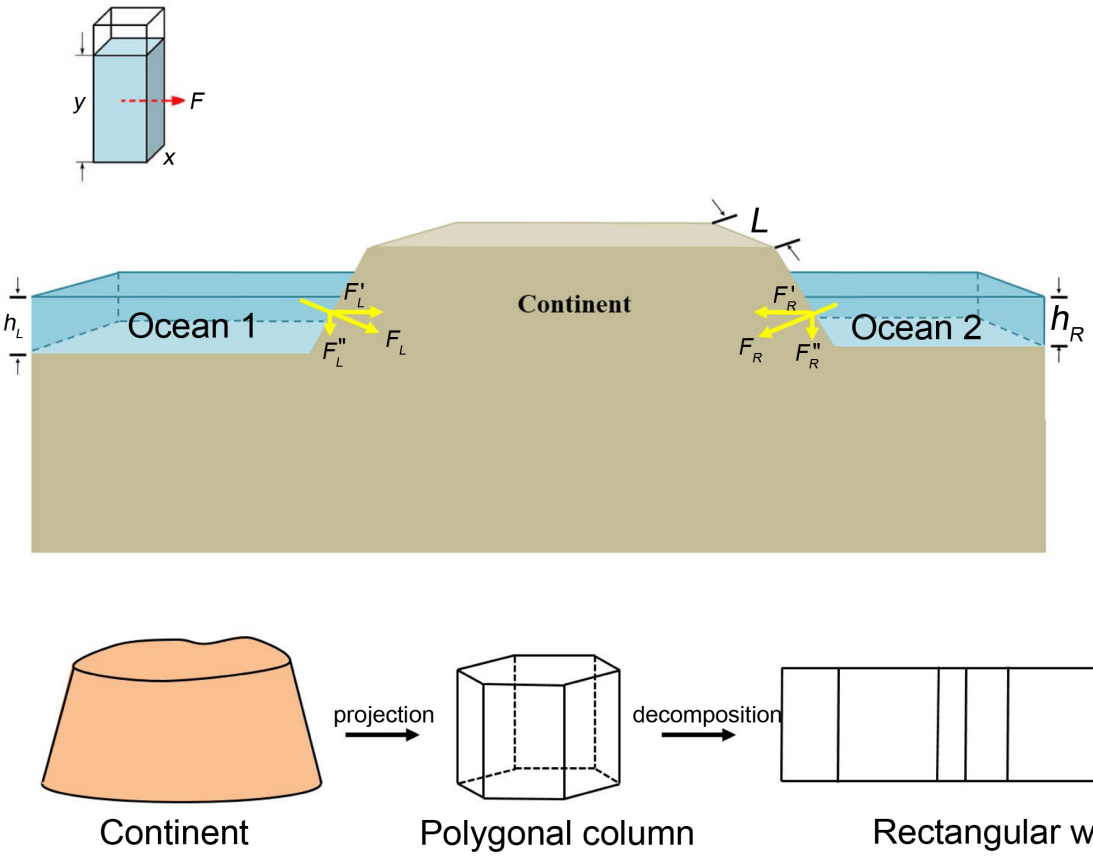


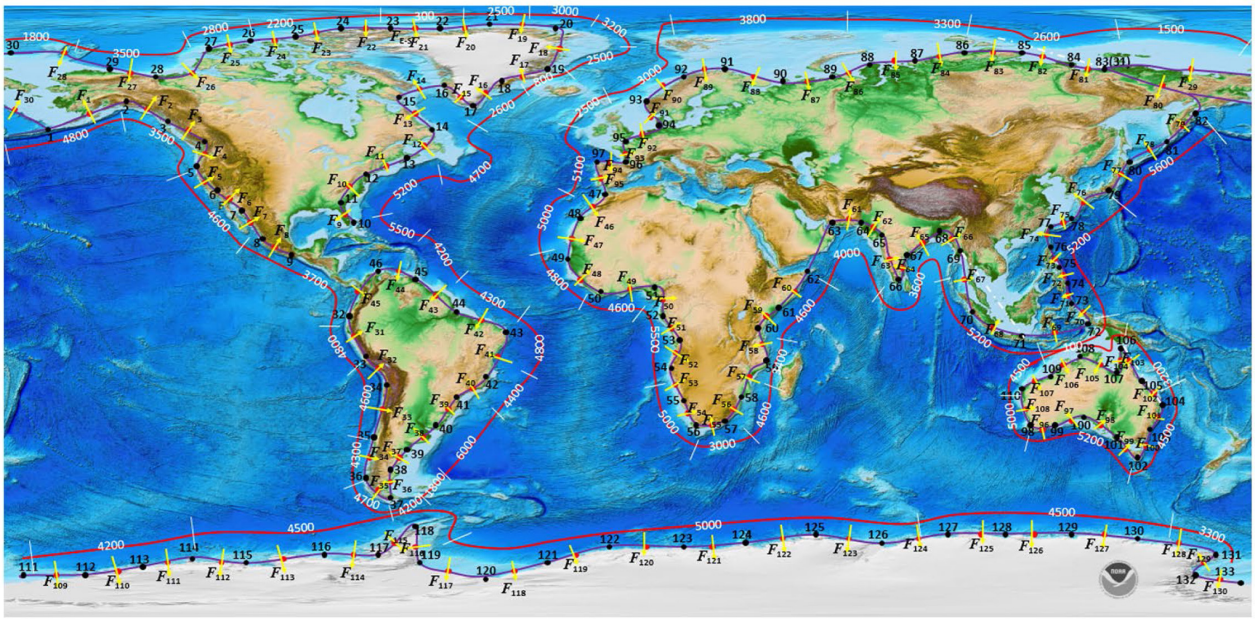

**Figure 2.** Top, conceptual model the ocean-generated forces acting on a straight continent. Middle, conceptual model of projecting continent into polygonal column and decomposing column into rectangular walls. Bottom, geographic treatment of the control sites and horizontal forces on the continents. $F$ (yellow arrows) denotes the horizontal force. The red lines and black dots denote the ocean depths and control sites, respectively; the red dots denote the geometric centers of the walls. The background map is from ETOPO1 Global Relief Model [8]. Note that the ocean depths were artificially resolved through the NOAA bathymetric data viewer.

**Table 1.** (a) The horizontal forces and the parameters for calculating them. (b) The horizontal forces and the parameters for calculating them (continued). (c) The horizontal forces and the parameters for calculating them (continued). (d) The horizontal forces and the parameters for calculating them (continued).

(a)

| Control site | | | Side | | | | | | |
|---|---|---|---|---|---|---|---|---|---|
| | | | | Length | Hypothetical geometric center | | Ocean depth | Horizontal force | |
| $j$ | $d_j$ | $q_j$ | $i$ | $L_i$ | $\alpha_i$ | $\beta_i$ | $h_{\text{i-ocean}}$ | $F_i$ | Inclination to latitude, east |
| | Longitude | Latitude | | km | Longitude | Latitude | m | N (*$10^{17}$) | Degrees (°) |
| 1 | 194.09˚ | 54.23˚ | 1 | 1747.90 | 204.23˚ | 60.39˚ | 4800 | 1.9733 | 140.74˚ |
| 2 | 214.37˚ | 66.55˚ | 2 | 1071.92 | 220.79˚ | 62.71˚ | 4800 | 1.2102 | 127.52˚ |
| 3 | 227.21˚ | 58.86˚ | 3 | 1190.03 | 232.02˚ | 54.29˚ | 3500 | 0.7143 | 121.53˚ |
| 4 | 236.82˚ | 49.71˚ | 4 | 931.50 | 236.29˚ | 45.54˚ | 3500 | 0.5591 | 354.92˚ |
| 5 | 235.76˚ | 41.36˚ | 5 | 921.16 | 238.93˚ | 38.05˚ | 4600 | 0.9551 | 36.94˚ |
| 6 | 242.09˚ | 34.73˚ | 6 | 1319.66 | 246.74˚ | 30.35˚ | 4600 | 1.3683 | 42.46˚ |
| 7 | 251.39˚ | 25.96˚ | 7 | 662.22 | 253.02˚ | 23.38˚ | 4000 | 0.5192 | 30.03˚ |
| 8 | 254.64˚ | 20.80˚ | 8 | 1092.31 | 259.13˚ | 18.34˚ | 3700 | 0.7327 | 59.98˚ |
| 9 | 263.61˚ | 15.88˚ | | | | | | | |
| 10 | 280.94˚ | 25.22˚ | 9 | 700.05 | 279.36˚ | 28.05˚ | 5500 | 1.0377 | 206.26˚ |
| 11 | 277.78˚ | 30.87˚ | 10 | 1125.90 | 281.21˚ | 35.10˚ | 5200 | 1.4918 | 146.46˚ |
| 12 | 284.63˚ | 39.32˚ | 11 | 1126.57 | 290.39˚ | 42.06˚ | 5200 | 1.4927 | 122.57˚ |
| 13 | 296.15˚ | 44.79˚ | 12 | 1032.68 | 300.23˚ | 48.58˚ | 5200 | 1.3683 | 144.54˚ |
| 14 | 304.31˚ | 52.37˚ | 13 | 1254.00 | 299.14˚ | 57.29˚ | 3000 | 0.5530 | 209.60˚ |
| 15 | 293.97˚ | 62.21˚ | 14 | 701.87 | 300.48˚ | 63.47˚ | 4700 | 0.7597 | 113.29˚ |
| 16 | 306.98˚ | 64.72˚ | 15 | 708.93 | 311.51˚ | 62.32˚ | 3000 | 0.3126 | 41.23˚ |
| 17 | 316.04˚ | 59.91˚ | 16 | 870.41 | 320.23˚ | 63.36˚ | 2600 | 0.2883 | 151.37˚ |
| 18 | 324.42˚ | 66.80˚ | 17 | 662.56 | 330.75˚ | 68.72˚ | 800 | 0.0208 | 129.72˚ |
| 19 | 337.08˚ | 70.63˚ | 18 | 1360.30 | 337.57˚ | 76.75˚ | 3200 | 0.6825 | 178.95˚ |
| 20 | 338.06˚ | 82.87˚ | 19 | 275.43 | 327.87˚ | 83.08˚ | 2800 | 0.1058 | 260.40˚ |
| 21 | 317.67˚ | 83.29˚ | 20 | 198.31 | 311.52˚ | 82.83˚ | 2500 | 0.0607 | 239.16˚ |
| 22 | 305.37˚ | 82.37˚ | 21 | 231.66 | 297.64˚ | 82.75˚ | 300 | 0.0010 | 249.11˚ |
| 23 | 289.90˚ | 83.12˚ | 22 | 238.55 | 281.92˚ | 82.74˚ | 2200 | 0.0566 | 249.47˚ |
| 24 | 273.94˚ | 82.36˚ | 23 | 336.45 | 267.96˚ | 81.15˚ | 2200 | 0.0798 | 322.66˚ |
| 25 | 261.98˚ | 79.94˚ | 24 | 294.67 | 255.30˚ | 79.43˚ | 2200 | 0.0699 | 292.70˚ |
| 26 | 248.62˚ | 78.91˚ | 25 | 313.81 | 244.23˚ | 77.84˚ | 2800 | 0.1206 | 319.08˚ |
| 27 | 239.83˚ | 76.77˚ | 26 | 997.49 | 229.64˚ | 73.31˚ | 3500 | 0.5987 | 319.52˚ |
| 28 | 219.44˚ | 69.84˚ | 27 | 523.95 | 212.59˚ | 70.37˚ | 3500 | 0.3145 | 257.09˚ |
| 29 | 205.73˚ | 70.90˚ | 28 | 753.32 | 195.39˚ | 72.17˚ | 3500 | 0.4522 | 291.66˚ |
| 30 | 185.05˚ | 73.44˚ | 29 | 1601.37 | 171.87˚ | 68.03˚ | 1500 | 0.1766 | 317.22˚ |
| 31 | 158.68˚ | 62.61˚ | 30 | 2225.18 | 176.39˚ | 58.42˚ | 50 | 0.0003 | 293.80˚ |

Notes: all geographic sites refer to **Figure 2**.

(b)

| Control site | | | Side | | | | | | |
|---|---|---|---|---|---|---|---|---|---|
| | | | | Length | Hypothetical geometric center | | Ocean depth | Horizontal force | |
| $j$ | $d_j$ | $q_j$ | $i$ | $L_i$ | $\alpha_i$ | $\beta_i$ | $h_{\text{i-ocean}}$ | $F_i$ | Inclination to latitude, east |
| | Longitude | Latitude | | km | Longitude | Latitude | m | N (*$10^{17}$) | Degrees |
| 32 | 278.96˚ | −2.20˚ | 31 | 1290.88 | 281.25˚ | −7.55˚ | 4800 | 1.4573 | 22.92˚ |
| 33 | 283.53˚ | −12.90˚ | 32 | 1163.08 | 286.57˚ | −17.26˚ | 4600 | 1.2059 | 33.59˚ |
| 34 | 289.60˚ | −21.62˚ | 33 | 1737.42 | 287.89˚ | −29.30˚ | 4600 | 1.8014 | 349.01˚ |
| 35 | 286.17˚ | −36.97˚ | 34 | 1405.78 | 284.78˚ | −43.22˚ | 4300 | 1.2737 | 350.81˚ |
| 36 | 283.39˚ | −49.46˚ | 35 | 876.16 | 287.57˚ | −52.48˚ | 4700 | 0.9484 | 40.11˚ |
| 37 | 291.74˚ | −55.50˚ | 36 | 977.06 | 291.92˚ | −51.11˚ | 1800 | 0.1551 | 181.43˚ |
| 38 | 292.09˚ | −46.71˚ | 37 | 731.33 | 294.03˚ | −43.73˚ | 1800 | 0.1161 | 154.87˚ |
| 39 | 295.96˚ | −40.75˚ | 38 | 1014.55 | 300.13˚ | −37.59˚ | 6000 | 1.7897 | 133.75˚ |
| 40 | 304.29˚ | −34.43˚ | 39 | 1161.02 | 307.71˚ | −30.12˚ | 6000 | 2.0480 | 145.55˚ |
| 41 | 311.13˚ | −25.81˚ | 40 | 1086.71 | 315.40˚ | −22.90˚ | 5200 | 1.4398 | 126.58˚ |
| 42 | 319.66˚ | −19.98˚ | 41 | 1571.58 | 322.47˚ | −13.46˚ | 4600 | 1.6295 | 157.31˚ |
| 43 | 325.28˚ | −6.93˚ | 42 | 1744.37 | 318.22˚ | −3.48˚ | 4300 | 1.5804 | 243.89˚ |
| 44 | 311.15˚ | −0.02˚ | 43 | 1602.67 | 305.40˚ | 4.36˚ | 4200 | 1.3853 | 232.65˚ |
| 45 | 299.64˚ | 8.73˚ | 44 | 292.31 | 300.11˚ | 7.50˚ | 4800 | 0.3300 | 200.75˚ |
| 46 | 300.58˚ | 6.27˚ | 45 | 2576.75 | 289.77˚ | 2.04˚ | 3700 | 1.7285 | 291.42˚ |
| 47 | 353.22˚ | 34.24˚ | 46 | 908.04 | 350.19˚ | 31.09˚ | 5000 | 1.1123 | 320.52˚ |
| 48 | 347.15˚ | 27.93˚ | 47 | 1462.59 | 345.17˚ | 21.61˚ | 5000 | 1.7917 | 343.79˚ |
| 49 | 343.19˚ | 15.29˚ | 48 | 1482.74 | 347.41˚ | 10.07˚ | 4800 | 1.6739 | 38.46˚ |
| 50 | 351.63˚ | 4.84˚ | 49 | 1689.12 | 359.25˚ | 5.29˚ | 4600 | 1.7514 | 93.36˚ |
| 51 | 6.87˚ | 5.73˚ | 50 | 898.57 | 8.32˚ | 1.96˚ | 4600 | 0.9317 | 20.99˚ |
| 52 | 9.77˚ | −1.82˚ | 51 | 1051.19 | 11.94˚ | −6.03˚ | 5500 | 1.5581 | 27.12˚ |
| 53 | 14.11˚ | −10.24˚ | 52 | 887.15 | 13.10˚ | −14.11˚ | 5500 | 1.3150 | 345.81˚ |
| 54 | 12.09˚ | −17.98˚ | 53 | 1157.53 | 14.03˚ | −22.88˚ | 5000 | 1.4180 | 19.99˚ |
| 55 | 15.96˚ | −27.77˚ | 54 | 779.24 | 17.82˚ | −30.90˚ | 5000 | 0.9546 | 26.98˚ |
| 56 | 19.67˚ | −34.02˚ | 55 | 669.59 | 23.27˚ | −33.69˚ | 3000 | 0.2953 | 83.72˚ |
| 57 | 26.87˚ | −33.36˚ | 56 | 1010.77 | 29.68˚ | −29.52˚ | 4600 | 1.0480 | 147.57˚ |
| 58 | 32.48˚ | −25.68˚ | 57 | 1416.91 | 36.40˚ | −20.46˚ | 4000 | 1.1109 | 144.93˚ |
| 59 | 40.31˚ | −15.24˚ | 58 | 1063.87 | 39.56˚ | −10.51˚ | 3400 | 0.6026 | 188.85˚ |
| 60 | 38.81˚ | −5.78˚ | 59 | 880.15 | 41.14˚ | −2.58˚ | 4600 | 0.9126 | 144.02˚ |
| 61 | 43.47˚ | 0.63˚ | 60 | 1479.88 | 47.38˚ | 6.04˚ | 4600 | 1.5344 | 144.34˚ |
| 62 | 51.29˚ | 11.45˚ | | | | | | | |

Notes: all geographic sites refer to **Figure 2**.

(c)

| Control site | | | Side | | | | | | |
|---|---|---|---|---|---|---|---|---|---|
| | | | | Length | Hypothetical geometric center | | Ocean depth | Horizontal force | |
| $j$ | $d_j$ | $q_j$ | $i$ | $L_i$ | $\alpha_i$ | $\beta_i$ | $h_{\text{i-ocean}}$ | $F_i$ | Inclination to latitude, east |
| | Longitude | Latitude | | km | Longitude | Latitude | m | N (*$10^{17}$) | Degrees |
| 69 | 95.41˚ | 16.55˚ | 67 | 1802.58 | 97.12˚ | 8.62˚ | 5000 | 2.2082 | 11.96˚ |
| 70 | 98.82˚ | 0.68˚ | 68 | 1806.5 | 105.79˚ | −3.54˚ | 5200 | 2.3935 | 60.27˚ |
| 71 | 112.76˚ | −7.75˚ | 69 | 2151.54 | 122.43˚ | −6.51˚ | 100 | 0.0011 | 97.36˚ |
| 72 | 132.09˚ | −5.27˚ | 70 | 1075.97 | 130.03˚ | −0.89˚ | 5200 | 1.4256 | 204.11˚ |
| 73 | 127.96˚ | 3.49˚ | 71 | 485.05 | 127.35˚ | 5.59˚ | 5200 | 0.6427 | 196.28˚ |
| 74 | 126.73˚ | 7.68˚ | 72 | 435.29 | 126.29˚ | 9.59˚ | 5200 | 0.5767 | 167.20˚ |
| 75 | 125.85˚ | 11.5˚ | 73 | 947.45 | 123.79˚ | 15.27˚ | 5200 | 1.2553 | 152.16˚ |
| 76 | 121.72˚ | 19.04˚ | 74 | 554.03 | 121.85˚ | 21.53˚ | 5200 | 0.7341 | 177.22˚ |
| 77 | 121.98˚ | 24.02˚ | 75 | 614.22 | 124.74˚ | 25.22˚ | 5200 | 0.8138 | 115.61 |
| 78 | 127.49˚ | 26.41˚ | 76 | 1399.63 | 132.94˚ | 30.63˚ | 5200 | 1.8545 | 131.96˚ |
| 79 | 138.39˚ | 34.84˚ | 77 | 1133.3 | 141.69˚ | 39.26˚ | 5600 | 1.7415 | 150.02˚ |
| 80 | 144.98˚ | 43.68˚ | 78 | 954.18 | 149.84˚ | 46.38˚ | 5600 | 1.4662 | 128.80˚ |
| 81 | 154.69˚ | 49.07˚ | 79 | 1196.64 | 159.22˚ | 53.76˚ | 5600 | 1.8388 | 150.27˚ |
| 82 | 163.74˚ | 58.44˚ | 80 | 1136.53 | 161.21˚ | 60.53˚ | 3800 | 0.8042 | 266.56˚ |
| 83 | 158.68˚ | 62.61˚ | 81 | 1393.86 | 143.60˚ | 67.44˚ | 1500 | 0.1537 | 254.05˚ |
| 84 | 128.51˚ | 72.26˚ | 82 | 603.43 | 120.52˚ | 73.84˚ | 2600 | 0.1999 | 234.78˚ |
| 85 | 112.52˚ | 75.42˚ | 83 | 469.11 | 104.03˚ | 75.62˚ | 2600 | 0.1554 | 275.25˚ |
| 86 | 95.54˚ | 75.81˚ | 84 | 440.81 | 89.21˚ | 74.73˚ | 3300 | 0.2352 | 302.95˚ |
| 87 | 82.88˚ | 73.64˚ | 85 | 490.57 | 75.85˚ | 72.86˚ | 3300 | 0.2618 | 290.54˚ |
| 88 | 68.82˚ | 72.08˚ | 86 | 529.37 | 63.55˚ | 70.47˚ | 3800 | 0.3746 | 312.33˚ |
| 89 | 58.27˚ | 68.86˚ | 87 | 603.56 | 51.38˚ | 68.00˚ | 3800 | 0.4271 | 288.45˚ |
| 90 | 44.49˚ | 67.13˚ | 88 | 546.62 | 38.16˚ | 67.67˚ | 3800 | 0.3868 | 257.5˚ |
| 91 | 31.83˚ | 68.20˚ | 89 | 753.91 | 23.04˚ | 67.60˚ | 3800 | 0.5334 | 280.17˚ |
| 92 | 14.25˚ | 66.99˚ | 90 | 733.5 | 9.68˚ | 64.34˚ | 300 | 0.0032 | 323.21˚ |
| 93 | 5.11˚ | 61.69˚ | 91 | 926.31 | 6.17˚ | 57.56˚ | 5100 | 1.1806 | 7.80˚ |
| 94 | 7.22˚ | 53.43˚ | 92 | 708.24 | 183.36˚ | 51.35˚ | 3000 | 0.3123 | 310.79˚ |
| 95 | 359.49˚ | 49.26˚ | 93 | 591.35 | 359.14˚ | 46.61˚ | 5100 | 0.7537 | 5.18˚ |
| 96 | 358.79˚ | 43.96˚ | 94 | 761.67 | 354.04˚ | 43.83˚ | 5100 | 0.9707 | 267.83˚ |
| 97 | 349.29˚ | 43.70˚ | 95 | 1104.32 | 351.26˚ | 38.97˚ | 5100 | 1.4074 | 17.89˚ |
| 98 | 133.29˚ | −38.42˚ | 96 | 1032.06 | 128.33˚ | −36.08˚ | 5200 | 1.3674 | 120.28˚ |
| 99 | 123.36˚ | −33.73˚ | 97 | 774.89 | 127.27˚ | −32.59˚ | 5200 | 1.0267 | 109.16˚ |
| 100 | 131.18˚ | −31.44˚ | 98 | 1089.81 | 135.80˚ | −34.55˚ | 5200 | 1.444 | 50.76˚ |
| 101 | 140.41˚ | −37.65˚ | 99 | 875.86 | 143.60˚ | −40.77˚ | 5200 | 1.1605 | 37.70˚ |
| 102 | 146.78˚ | −43.89˚ | 100 | 958.73 | 148.49˚ | −39.78˚ | 4500 | 0.9513 | 162.28˚ |
| 103 | 150.20˚ | −35.67˚ | 101 | 877.51 | 152.09˚ | −32.06˚ | 4500 | 0.8707 | 156.08˚ |
| 104 | 153.98˚ | −28.45˚ | 102 | 943.16 | 151.56˚ | −24.82˚ | 3200 | 0.4732 | 211.22˚ |

Notes: all geographic sites refer to **Figure 2**.

(d)

| Control site | | | Side | | | | | | |
|---|---|---|---|---|---|---|---|---|---|
| | | | | Length | Hypothetical geometric center | | Ocean depth | Horizontal force | |
| $j$ | $d_j$ | $q_j$ | $i$ | $L_i$ | $\alpha_i$ | $\beta_i$ | $h_{i\text{-ocean}}$ | $F_i$ | Inclination to latitude, east |
| | Longitude | Latitude | | km | Longitude | Latitude | m | N (*1017) | Degrees |
| 105 | 149.13˚ | −21.19˚ | 103 | 1359.76 | 145.75˚ | −16.01˚ | 3200 | 0.6823 | 212.08˚ |
| 106 | 142.36˚ | −10.82˚ | 104 | 802.72 | 141.57˚ | −14.35˚ | 100 | 0.0004 | 347.77˚ |
| 107 | 140.78˚ | −17.88˚ | 105 | 1216.8 | 135.51˚ | −15.81˚ | 100 | 0.0006 | 247.79˚ |
| 108 | 130.24˚ | −13.74˚ | 106 | 1109.61 | 125.89˚ | −16.48˚ | 100 | 0.0005 | 303.28˚ |
| 109 | 121.53˚ | −19.22˚ | 107 | 864.63 | 117.80˚ | −20.95˚ | 4500 | 0.8579 | 296.31˚ |
| 110 | 114.06˚ | −22.67˚ | 108 | 2529.37 | 123.68˚ | −30.55˚ | 5000 | 3.0985 | 46.39˚ |
| 111 | 188.47˚ | −78.56˚ | 109 | 391.5 | 196.72˚ | −78.09˚ | 4200 | 0.3384 | 285.48˚ |
| 112 | 204.97˚ | −77.61˚ | 110 | 519.06 | 213.35˚ | −76.35˚ | 4200 | 0.4487 | 302.42˚ |
| 113 | 221.73˚ | −75.08 | 111 | 461.58 | 229.17˚ | −74.47˚ | 4200 | 0.399 | 286.94˚ |
| 114 | 236.61˚ | −73.86˚ | 112 | 401.97 | 243.06˚ | −74.38˚ | 4500 | 0.3989 | 253.39˚ |
| 115 | 249.51˚ | −74.90˚ | 113 | 780.47 | 261.99˚ | −74.03˚ | 4500 | 0.7744 | 284.02˚ |
| 116 | 274.46˚ | −73.16˚ | 114 | 477.75 | 281.74˚ | −72.91˚ | 4500 | 0.4741 | 263.24˚ |
| 117 | 289.02˚ | −72.65˚ | 115 | 1595.2 | 298.54˚ | −66.48˚ | 4500 | 1.5828 | 328.21˚ |
| 118 | 308.06˚ | −60.30˚ | 116 | 1702.14 | 305.75˚ | −67.92˚ | 5000 | 2.0851 | 186.49˚ |
| 119 | 303.40˚ | −75.53˚ | 117 | 418.96 | 309.48˚ | −76.83˚ | 5000 | 0.5132 | 226.90˚ |
| 120 | 315.53˚ | −78.12˚ | 118 | 850.21 | 327.66˚ | −75.67˚ | 5000 | 1.0415 | 308.82˚ |
| 121 | 339.79˚ | −73.22˚ | 119 | 644.56 | 347.35˚ | −71.56˚ | 5000 | 0.7896 | 304.72˚ |
| 122 | 354.90˚ | −69.89˚ | 120 | 919.54 | 186.86˚ | −69.65˚ | 5000 | 1.1264 | 266.74˚ |
| 123 | 18.81˚ | −69.41˚ | 121 | 674.24 | 26.90˚ | −68.64˚ | 5000 | 0.8259 | 284.57˚ |
| 124 | 34.98˚ | −67.87˚ | 122 | 819.5 | 44.05˚ | −66.87˚ | 5000 | 1.0039 | 285.64˚ |
| 125 | 53.12˚ | −65.86˚ | 123 | 838.69 | 62.26˚ | −67.22˚ | 5000 | 1.0274 | 249.11˚ |
| 126 | 71.40˚ | −68.58˚ | 124 | 983.34 | 82.48˚ | −67.32˚ | 5000 | 1.2046 | 286.27˚ |
| 127 | 93.55˚ | −66.06˚ | 125 | 675.92 | 101.11˚ | −66.29˚ | 4500 | 0.6707 | 265.79˚ |
| 128 | 108.67˚ | −66.51˚ | 126 | 908.21 | 119.04˚ | −66.82˚ | 4500 | 0.9012 | 267.30˚ |
| 129 | 129.41˚ | −66.90˚ | 127 | 654.62 | 136.97˚ | −67.01˚ | 4500 | 0.6495 | 267.88˚ |
| 130 | 144.52˚ | −67.12˚ | 128 | 1098.65 | 157.08˚ | −69.49˚ | 3900 | 0.8188 | 242.07˚ |
| 131 | 169.63˚ | −71.85˚ | 129 | 631.15 | 166.64˚ | −74.58˚ | 3300 | 0.3368 | 163.76˚ |
| 132 | 163.65˚ | −77.31˚ | 130 | 645.18 | 177.36˚ | −78.01˚ | 3300 | 0.3443 | 256.53˚ |
| 133 | 191.07˚ | −78.70˚ | | | | | | | |

Notes: all geographic sites refer to **Figure 2**.

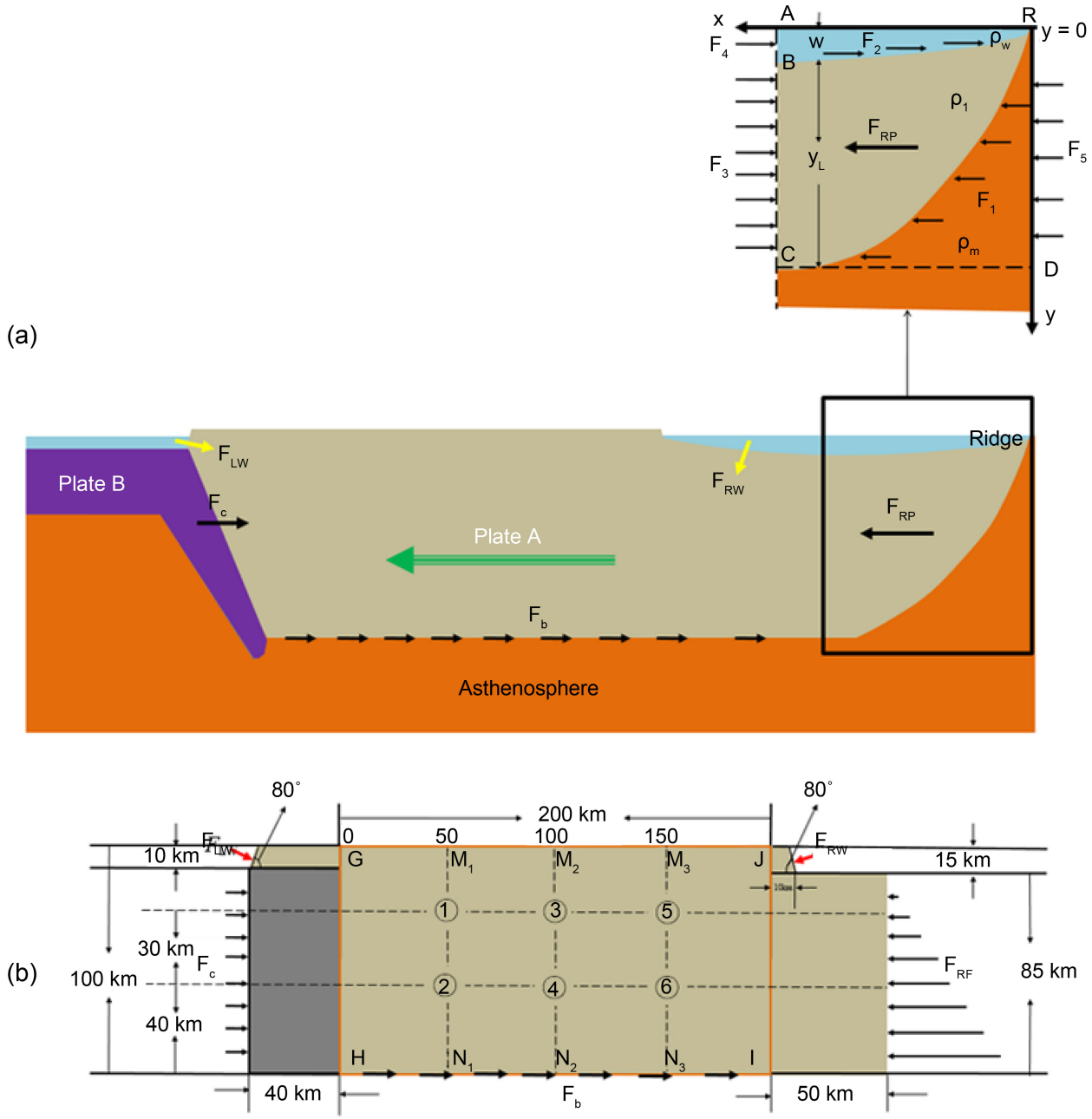


**Figure 3.** Conceptual model of the geodynamics around a continental plate (a) and simplified model for determining stress (b). $F_{RP}$, $F_b$, $F_c$, and $F_{LW}$($F_{RW}$) denote ridge push, basal friction, collisional, and ocean-generated forces.

to represent stress with this geometry. To overcome this shortage, we develop a simplified model (see Figure 3(b)) consisting of rocks that are straight. The model assumes homogeneity and isotropy and has a length and thickness of 290 km and 100 km, respectively.

### 4.1. Combined A

The ridge push force ($F_{RF}$), the collisional force ($F_c$), and the basal friction force ($F_b$) are included alone. This combination follows previous studies [10]-[12].

Along the horizontal direction, the ridge push force ($F_{RF}$) is driving and its amplitude increases with depth; the collisional force ($F_c$) is uniformly exerted on its left side; the mantle exerts a frictional force ($F_b$) on its base, and this force is resistive. These forces realize a force balance for the plate. Along the vertical direction, the model's weight is balanced out by the supporting from the mantle. We employ finite element analysis software (*i.e.*, Abaqus) to calculate the stresses yielded by these forces. The model's bottom is given a remote boundary condition. As the upper part of the lithospheric plate is brittle and elastic, whereas the lower part is ductile and plastic, we assume that the physical property of the rock is vertically transited from elasticity to plasticity. The inputs include the vertical pressure yielded by the rock's weight and the lateral pressures yielded by these forces ($F_{RF}$, $F_b$, and $F_c$). The outputs include the stresses caused by the vertical pressure alone and the stresses caused by a combination of the vertical and lateral pressures. The two-dimensional frame allows us to obtain a horizontal stresses (S11) and a vertical stresses (S22). We here only discuss the horizontal stress (S11). The elastic modulus, Poisson ratio, and rock density of the model are set to 100,000 MPa, 0.3, and 2690 kg/m$^3$, respectively. The vertical pressure caused by the rock's weight yields Set I data of stress; The $F_{RF}$ is given as $4.0 \times 10^{12}$ N m$^{-1}$, which is generally accepted by scientific community [9]. It is assumed that $F_b$ and $F_c$ are 80% and 20% of $F_{RF}$, respectively. The pressures caused by a combination of these forces yield Set II data of stress; In order to test the stress variation when the resistive forces are moderately changed, we again assume that $F_b$ and $F_c$ are 50% and 50% of $F_{RF}$, respectively. The pressures caused by a combination of these revised forces yield Set III data of stress. A detailed description of these forces for different sets is listed in Table 2.

Table 2. Different forces exerted on the model.

| Combination | No. | Loads (*$10^{12}$ N/m) | | | | |
|---|---|---|---|---|---|---|
| | | $F_{RP}$ | $F_b$ | $F_c$ | $F_{RW}$ | $F_{LW}$ |
| 1 | Set I | - | - | - | - | - |
| | Set II | 4.00 | 3.20 | 0.80 | - | - |
| | Set III | 4.00 | 2.00 | 2.00 | - | - |
| | Set II' | 200.00 | 160.00 | 40.00 | - | - |
| | Set III' | 200.00 | 100.00 | 100.00 | - | - |
| 2 | Set A | 4.00 | 3.21 | 0.87 | 0.12 | 0.04 |
| | Set B | 4.00 | 2.00 | 2.08 | 0.12 | 0.04 |
| | Set C | 0.04 | 0.03 | 0.09 | 0.12 | 0.04 |
| | Set D | 0.04 | 0.02 | 0.10 | 0.12 | 0.04 |
| | Set A' | 200.00 | 160.18 | 43.74 | 6.13 | 2.21 |
| | Set B' | 200.00 | 100.00 | 103.92 | 6.13 | 2.21 |
| | Set C' | 2.00 | 1.60 | 4.32 | 6.13 | 2.21 |
| | Set D' | 2.00 | 1.00 | 4.92 | 6.13 | 2.21 |

To realize a more accurate understanding of the resultant stress, we select a rectangular area *GHIJ* to exhibit. The stress clouds of this area are compared in **Figure 4(left)**. Please note that any of these forces ($F_{RF}$, $F_b$, and $F_c$) is too small with respect to the rock's weight. For instance, when $F_{RF} = 4.0 \times 10^{12}$ N m$^{-1}$ is applied to the model's right side (which is 85 km length), its resultant mean pressure is 47.06 MPa, while the mean lithostatic pressure of the rock in the model (which is 100 km depth) is 1318.1 MPa. This means that, if we use stress cloud to compare the stress caused by a combination of the rock's weight and these forces with the stress caused by the rock's weight alone, the two are indistinguishable. To create a visual impression, we magnify these forces ($F_{RF}$, $F_b$, and $F_c$) 50 times, which yields Set II' data of stress and Set III' data of stress. Clearly, we find that the horizontal stresses caused by these forces are compressional and mainly concentrated on the lower part of section *GHIJ*. Three sections ($M_1N_1$, $M_2N_2$, and $M_3N_3$) in the rectangular area are extracted to quantify the comparison. Each section keeps a span of 50 km relative to one another. The stress diagrams for these sections are compared in **Figure 4(right)**. After subtracting the stresses caused by the rock's weight from the stresses caused by a combination of the rock's weight and these forces, we obtain the stresses caused by these forces, which is exhibited in Set II (III) - Set I.

Kusznir and Bott [13] argued that, due to the ductile nature of the lower part of the lithosphere, there would be a redistribution of any stress applied to the whole lithosphere that would result in stress amplification in the upper brittle part of the lithosphere. This view is based on the assumption that force is uniformly exerted on the side of the lithospheric plate, but reality is that the ridge push force increases with depth; consequently, the redistribution of the resultant stress and its amplification are not applicable. In contrast, we have considered this ductile nature in the modelling, but no evidence was found for stress amplification in the upper part of section *GHIJ*. Our modelling suggests that the stresses caused by a combination of the ridge push, collisional, and basal friction forces are mainly concentrated on the lower part of the lithosphere, this feature doesn't accord with the observed stresses that are mainly concentrated on the uppermost brittle part of the lithosphere (which is ~40 km in depth) [10] [14] [15].

### 4.2. Combined B

The ocean-generated forces ($F_{LW}$ and $F_{RW}$), the ridge push force ($F_{RF}$), the collisional force ($F_c$), and the basal friction force ($F_b$) are included. The inputs include the vertical pressure caused by the rock's weight and the lateral pressures caused by these forces ($F_{RW}$, $F_{LW}$, $F_{RF}$, $F_c$, and $F_b$). The ocean-generated forces $F_{LW}$ and $F_{RW}$ correspond to 5 km water depth at the right and 3 km water depth at the left, respectively, and $F_{RW} = 0.12 \times 10^{12}$ N m$^{-1}$, $F_{LW} = 0.04 \times 10^{12}$ N m$^{-1}$. The outputs include the stresses yielded by the vertical pressure alone and the stresses yielded by a combination of the vertical and lateral pressures. Similarly, we only discuss the horizontal stress (S11). At this time, we first use these forces to yield Set A data

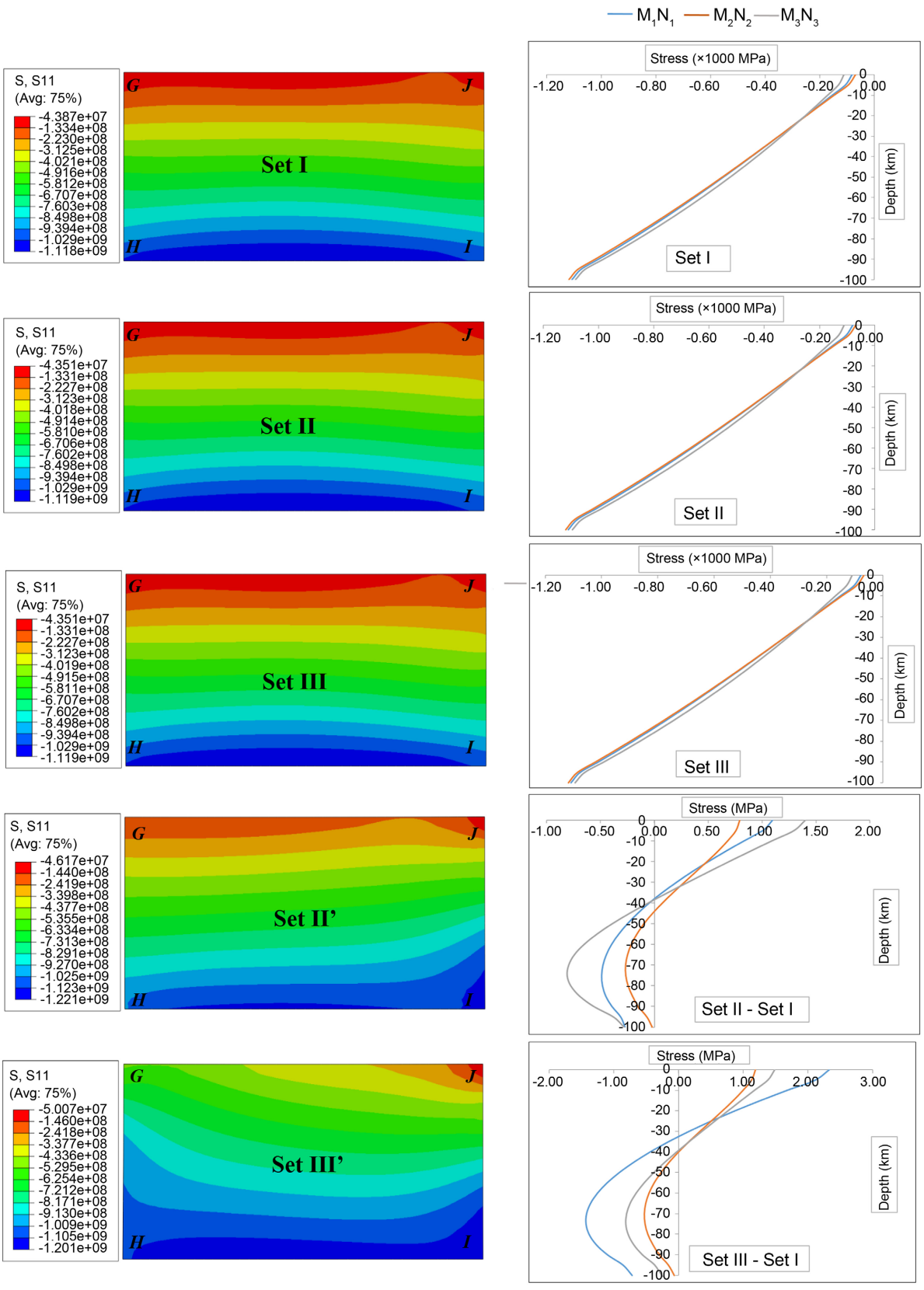


**Figure 4.** Stress clouds (left) and diagrams (right) produced by the rock's weight, ridge push, basal friction, and collisional forces. "–" denotes the stresses are compressional, whereas "+" denotes the stresses are tensional.

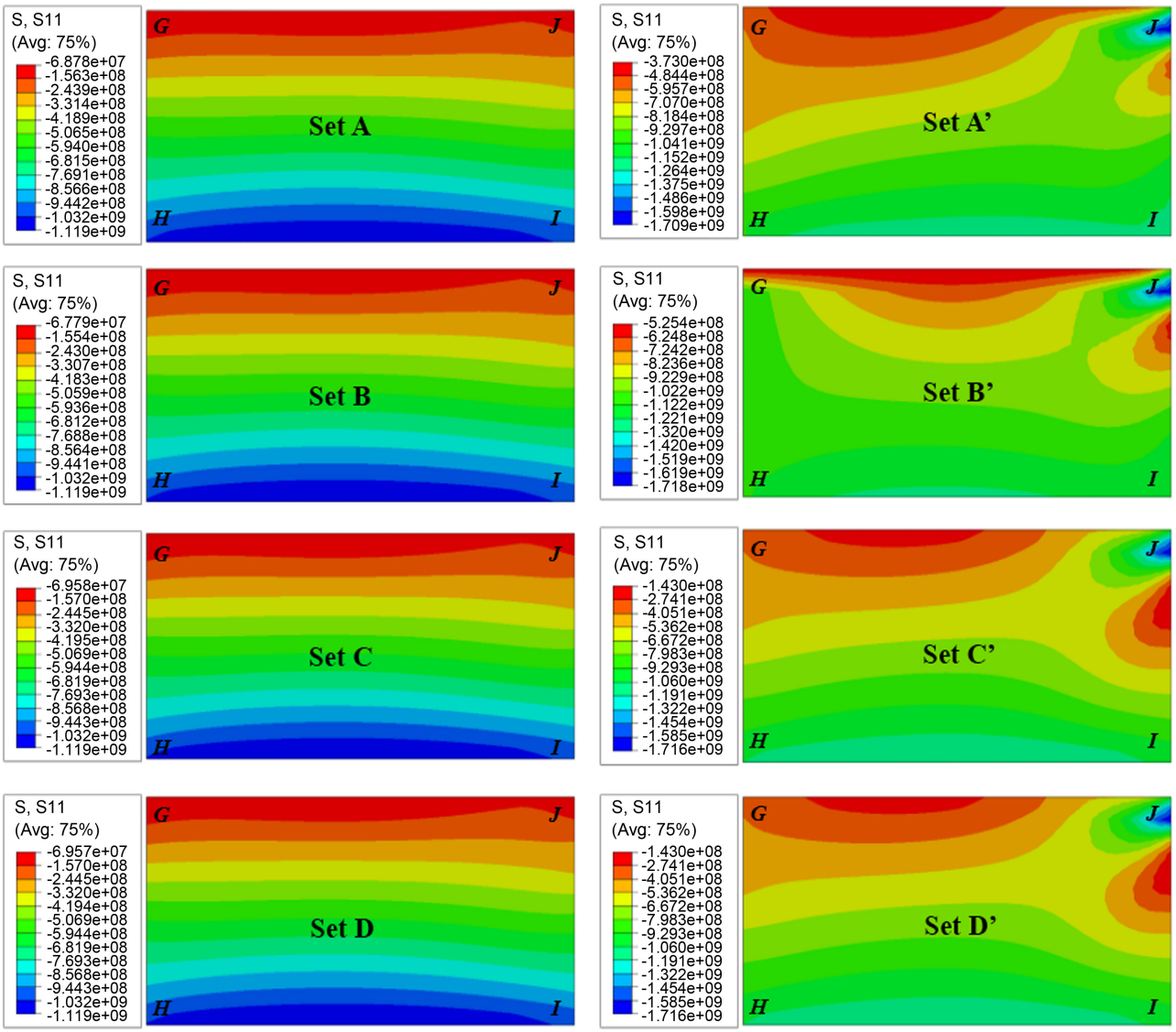


**Figure 5.** Stress clouds (left) and diagrams (right) produced by the ocean-generated force, ridge push force, basal friction, and collisional forces. "–" denotes compressional stress, whereas "+" denotes tensional stress.

of stress and Set B data of stress. The stress clouds of the area *GHIJ* are compared in Figure 5. To realize a visual impression, we magnify these forces ($F_{RW}$, $F_{LW}$, $F_{RF}$, $F_c$, and $F_b$) 50 times, which yields Set A' data of stress and Set B' data of stress. We find that the horizontal stresses caused by these forces are compressional and tend to distribute across the middle part of section *GHIJ*. We then minify $F_{RF}$ and $F_b$ 100 times, remain $F_{RW}$ and $F_{LW}$ stable, and adjust $F_c$ properly so as to sustain the horizontal force balance, this yields Set C data of stress and Set D data of stress. To realize a visual impression, we again magnify these revised forces 50 times, which yields Set C' data of stress and Set D' data of stress. A detailed description of these forces for different sets is listed in Table 2. It can be found that, after $F_{RF}$ and $F_b$ are reduced, the horizontal stresses caused by these forces are mostly concentrated on the upper part of section *GHIJ*. The stress diagrams for three sections

(*i.e.*, $M_1N_1$, $M_2N_2$, and $M_3N_3$) are counted and compared in **Figure 6**. After subtracting the stresses caused by the rock's weight, we obtain the stresses caused by these forces, which are exhibited with Set A/B/C/D - Set I. We find that the stresses caused by a combination of the ocean-generated, ridge push (when its amplitude is lowered to be less than that of the ocean-generated force), collisional, and basal friction forces are mostly concentrated on the upper part of the lithosphere. This distribution feature accords with that of observed stresses [10] [14] [15].

### 4.3. Combined C

The ocean-generated forces ($F_{LW}$ and $F_{RW}$) including the effect of tide, the ridge push force ($F_{RF}$), the collisional force ($F_c$), and the basal friction force ($F_b$) are included. The inputs include the vertical pressure caused by the rock's weight and the lateral pressures caused by these forces ($F_{RW}$, $F_{LW}$, $F_{RP}$, $F_b$, and $F_c$). Since tide represents a periodic oscillation, we design a water level variation of totally 12 hours, which corresponds to a semidiurnal tide. The information of tidal height and these forces is listed in **Table 3**. The outputs include the stresses produced by the vertical pressure alone and the stresses produced by a combination of the vertical and lateral pressures. Using the latter to subtract the former, we obtain the stresses produced by the lateral pressures. Similarly, we only discuss the horizontal stress (S11). At this time, we collect the results of 6 locations (①, ②, ③, ④, ⑤, and ⑥), as shown in **Figure 3(b)**, to do comparison. These locations belong to the 30 km depth and 60 km depth of three sections ($M_1N_1$, $M_2N_2$, and $M_3N_3$) in the model. The stress diagrams for these locations are compared in **Figure 7**. The stresses exhibited in **Figure 7(A)** are that produced by the vertical pressure alone, the stresses exhibited in **Figure 7(B)** are that produced by a combination of the vertical and lateral pressures, and the stresses exhibited in **Figure 7(B-A)** is that produced by the lateral pressures.

As exhibited in Set C(D) - Set I of **Figure 6**, the horizontal stresses yielded by the ocean-generated force may have penetrated a 50 km depth crust, which represents mostly continent, and their amplitude is approximately 2.0 - 6.0 MPa, which is entirely comparable to the range of earthquake stress drops (1 - 30 Mpa) [16]. Our model assumes homogenous and isotropic rocks in a straight configuration, whereas the actual Earth's crust is spatially curved, and the crustal rocks within it are inhomogeneous and anisotropic. Most importantly, ocean water has been exerting on the Earth's crust for more than 4 billion years [4]-[6], and based on the elastic rebound theory for earthquakes [17], stress is time-dependent and tends to accumulate gradually. From these points, we expect that the actual stress in the Earth's crust due to ocean-generated force may have been higher than that we have modelled here. It is important to note that our modeling is not yet capable of quantitatively comparing with the observed stress. This limitation stems from two primary factors. Firstly, as highlighted by Morawietz *et al.* [18], while the World Stress Map project [14] [19] has consistently released data, these primarily encompass stress orientations and patterns (*i.e.*, compressional and extensional),

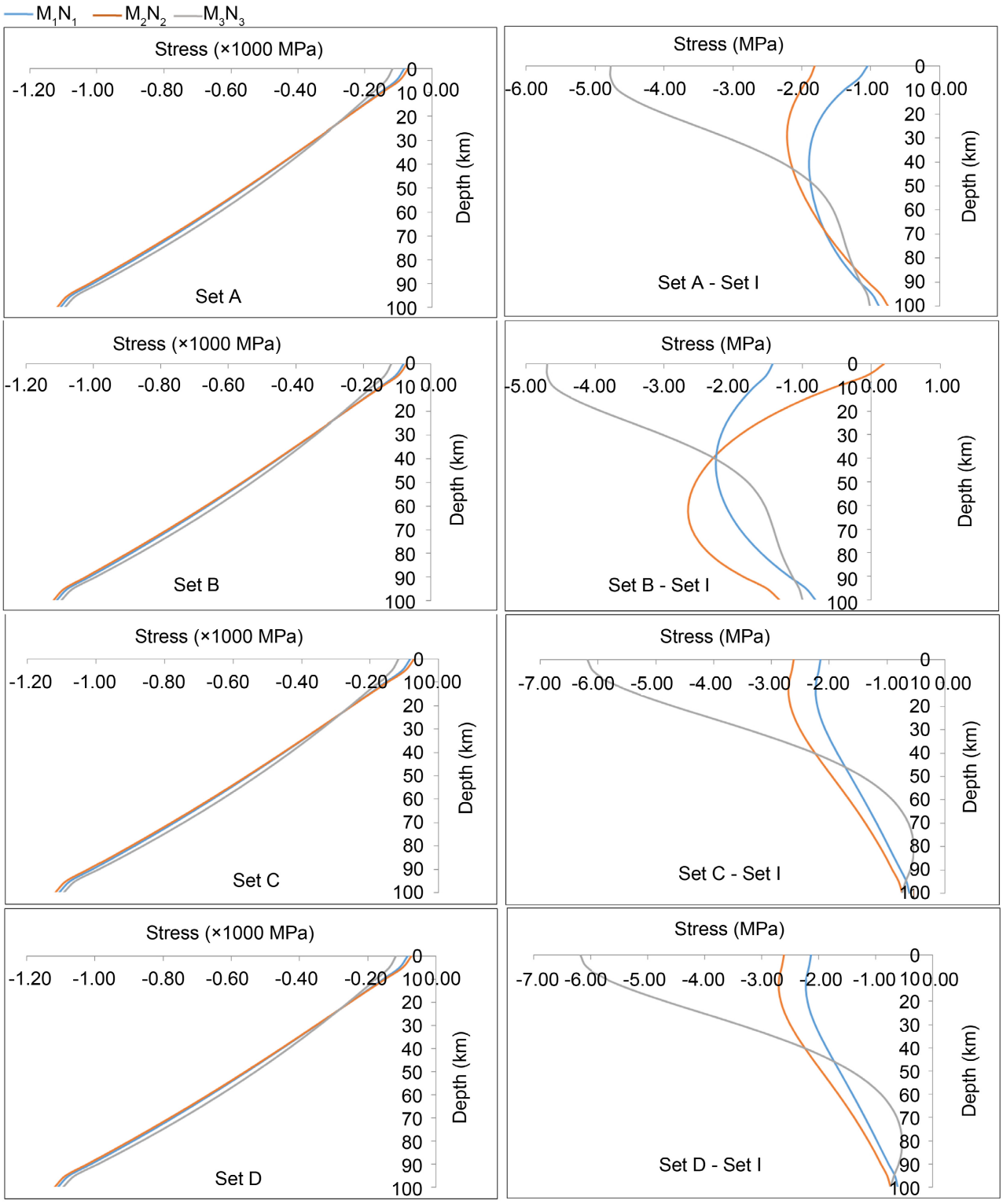


**Figure 6.** Stress diagram produced by the ocean-generated, ridge push force, basal friction, and collisional forces. "–" denotes compressional stress, whereas "+" denotes tensional stress.

excluding the magnitude of stress. Secondly, the locally acquired stress magnitude data in Germany and neighboring regions are confined to a shallow depth (less

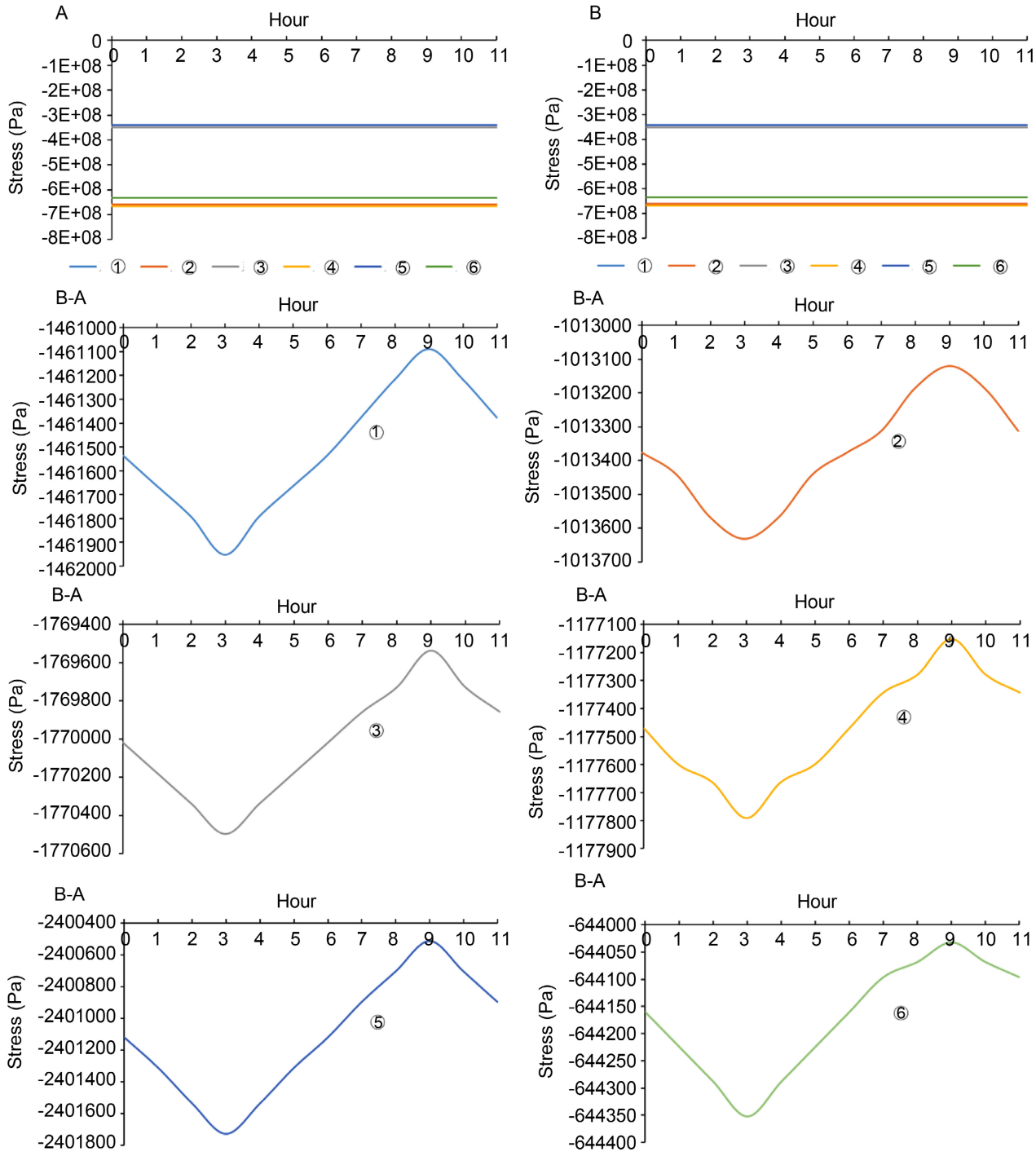


**Figure 7.** The stress variation due to tide. Note, the stress variations in A and B are too small to be perceptible.

than 7.0 km beneath the Earth's surface). Within this depth, the stresses generated are significantly influenced by the inhomogeneous and anisotropic characteristics of rock materials, which cannot be fully captured by our model. Even so, our model is providing a new starting point for scientific community to address this intricate issue.

**Table 3.** Information of tidal height and related forces around the model.

| Time (h) | Tidal height (m) | Loads ($\times 10^{11}$ N/m) | | | | |
|---|---|---|---|---|---|---|
| | | $F_{LW}$ | $F_{RW}$ | $F_{RP}$ | $F_b$ | $F_c$ |
| 0 | 0.0 | 0.4410000000 | 1.2250000000 | 0.4000000000 | 0.2000000000 | 1.0000000000 |
| 1 | 0.4 | 0.4411176078 | 1.2251960078 | 0.4000000000 | 0.2000000000 | 1.0000000000 |
| 2 | 0.8 | 0.4412352314 | 1.2253920314 | 0.4000000000 | 0.2000000000 | 1.0000000000 |
| 3 | 1.2 | 0.4413528706 | 1.2255880706 | 0.4000000000 | 0.2000000000 | 1.0000000000 |
| 4 | 0.8 | 0.4412352314 | 1.2253920314 | 0.4000000000 | 0.2000000000 | 1.0000000000 |
| 5 | 0.4 | 0.4411176078 | 1.2251960078 | 0.4000000000 | 0.2000000000 | 1.0000000000 |
| 6 | 0.0 | 0.4410000000 | 1.2250000000 | 0.4000000000 | 0.2000000000 | 1.0000000000 |
| 7 | −0.4 | 0.4408824078 | 1.2248040078 | 0.4000000000 | 0.2000000000 | 1.0000000000 |
| 8 | −0.8 | 0.4407648314 | 1.2246080314 | 0.4000000000 | 0.2000000000 | 1.0000000000 |
| 9 | −1.2 | 0.4406472706 | 1.2244120706 | 0.4000000000 | 0.2000000000 | 1.0000000000 |
| 10 | −0.8 | 0.4407648314 | 1.2246080314 | 0.4000000000 | 0.2000000000 | 1.0000000000 |
| 11 | −0.4 | 0.4408824078 | 1.2248040078 | 0.4000000000 | 0.2000000000 | 1.0000000000 |

## 5. Discussion

The coupling of water and earthquake occurrence is a highly active area of research, with reservoir-induced earthquakes being the most notable artificial seismicity events. It has been extensively reported that there have been hundreds of instances, including at least five sites, where earthquakes exceeding M 6 have occurred [20], indicating that earthquakes near reservoirs are widespread [21] [22]. The primary process for reservoir-induced earthquakes is a stress change within rocks due to the water loading [21] [23], and the frequencies of these earthquakes closely correlate with the loading and unloading rate of water [24] [25]. These authors [26]-[28] have theorized/modelled the link between seismicity and stress caused by reservoir water impoundment. In addition to these reservoir-induced earthquakes, ocean water-related earthquakes were also recently reported. Guillas *et al.* [29] identified a connection between the El Niño-Southern Oscillation (ENSO) and earthquakes on the East Pacific Rise (EPR), proposing that seismicity may increase due to a reduction in ocean-bottom pressure over the EPR. Martínez-Garzón *et al.* [30] discovered that changes in sea level affect seismicity rates in a hydrothermal system near Istanbul. Tanaka *et al.* [31] concluded that the most likely component to control the earthquake occurrence is the stress. As exhibited in **Figure 7**, the stress variation caused by the tide may have penetrated a 50 km depth crust. The result of our modelling, combined with these existing understanding of reservoir-induced and ocean water-related earthquakes, leads us to speculate that the ocean-generated force may potentially contribute to earthquake occurrence, although integrate data (*i.e.*, seismic events and oceanic pressure measurements) to support this coupling are still waited.

## Acknowledgements

We express sincere thanks to John M. Cimbala, Chris Hughes, and Gerald Shubert for their comments on the force between ocean and continent. The author declares no conflicts of interest. This research received no funding.

## Data Availability Statement

The latitude and longitude of the controlling sites on the continental plates in **Figure 2** are determined through the ETOPO1 Global Relief Model [8], and the ocean depths are artificially resolved through the NOAA Bathymetric Data Viewer (https://ngdc.noaa.gov/mgg/global/global.html).

## Conflicts of Interest

The author declares no conflicts of interest regarding the publication of this paper.

## References

[1] Cawood, P.A., Hawkesworth, C.J. and Dhuime, B. (2012) The Continental Record and the Generation of Continental Crust. *Geological Society of America Bulletin*, **125**, 14-32. https://doi.org/10.1130/b30722.1

[2] Wang, Y., Jian, Z., Zhao, P., Xiao, D. and Chen, J. (2016) Relative Roles of Land- and Ocean-Atmosphere Interactions in Asian-Pacific Thermal Contrast Variability at the Precessional Band. *Scientific Reports*, **6**, Article No. 28349. https://doi.org/10.1038/srep28349

[3] Cameselle, A.L., Ranero, C.R., Franke, D. and Barckhausen, U. (2015) The Continent-ocean Transition on the Northwestern South China Sea. *Basin Research*, **29**, 73-95. https://doi.org/10.1111/bre.12137

[4] Bercovici, D., Tackley, P.J. and Ricard, Y. (2015) The Generation of Plate Tectonics from Mantle Dynamics. In: Schubert, G., Ed., *Treatise on Geophysics*, Elsevier, 271-318. https://doi.org/10.1016/b978-0-444-53802-4.00135-4

[5] Mojzsis, S.J., Harrison, T.M. and Pidgeon, R.T. (2001) Oxygen-Isotope Evidence from Ancient Zircons for Liquid Water at the Earth's Surface 4,300 Myr Ago. *Nature*, **409**, 178-181. https://doi.org/10.1038/35051557

[6] Valley, J.W., Peck, W.H., King, E.M. and Wilde, S.A. (2002) A Cool Early Earth. *Geology*, **30**, 351-354. https://doi.org/10.1130/0091-7613(2002)030<0351:acee>2.0.co;2

[7] Cengel, Y.A. and Cimbala, J.M. (2017) Fluid Mechanics: Fundamentals and Applications. 4th Edition, McGraw-Hill Education.

[8] Amante, C. and Eakins, B.W. (2009) ETOPO1 1 Arc-Minute Global Relief Model: Procedures, Data Sources and Analysis. NOAA Technical Memorandum NESDIS NGDC-24, National Geophysical Data Center, NOAA. https://doi.org/10.7289/V5C8276M

[9] Turcotte, D. and Schubert, G. (2014). Geodynamics. 3rd Edition, Cambridge University Press. https://doi.org/10.1017/cbo9780511843877

[10] Zoback, M.L. (1992) First- and Second-Order Patterns of Stress in the Lithosphere: The World Stress Map Project. *Journal of Geophysical Research*: *Solid Earth*, **97**, 11703-11728. https://doi.org/10.1029/92jb00132

[11] Müller, B., Zoback, M.L., Fuchs, K., Mastin, L., Gregersen, S., Pavoni, N., *et al.* (1992) Regional Patterns of Tectonic Stress in Europe. *Journal of Geophysical Research*:

*Solid Earth*, **97**, 11783-11803. https://doi.org/10.1029/91jb01096

[12] Richardson, R.M. (1992) Ridge Forces, Absolute Plate Motions, and the Intraplate Stress Field. *Journal of Geophysical Research*: *Solid Earth*, **97**, 11739-11748. https://doi.org/10.1029/91jb00475

[13] Kusznir, N.J. and Bott, M.H.P. (1977) Stress Concentration in the Upper Lithosphere Caused by Underlying Visco-Elastic Creep. *Tectonophysics*, **43**, 247-256. https://doi.org/10.1016/0040-1951(77)90119-6

[14] Zoback, M.L., Zoback, M.D., Adams, J., Assumpção, M., Bell, S., Bergman, E.A., *et al.* (1989) Global Patterns of Tectonic Stress. *Nature*, **341**, 291-298. https://doi.org/10.1038/341291a0

[15] Zoback, M.L. and Magee, M. (1991) Stress Magnitudes in the Crust: Constraints from Stress Orientation and Relative Magnitude Data. *Philosophical Transactions of the Royal Society*, **A337**, 181-194.

[16] Kanamori, H. (1994) Mechanics of Earthquakes. *Annual Review of Earth and Planetary Sciences*, **22**, 207-237. https://doi.org/10.1146/annurev.ea.22.050194.001231

[17] Reid, H.F. (1910) The Mechanism of the Earthquake. In: T*he California Earthquake of April* 19, 1906. *Report of the State Earthquake Investigation Commission*, Carnegie Institution, 192.

[18] Morawietz, S., Heidbach, O., Reiter, K., Ziegler, M., Rajabi, M., Zimmermann, G., *et al.* (2020) An Open-Access Stress Magnitude Database for Germany and Adjacent Regions. *Geothermal Energy*, **8**, Article No. 25. https://doi.org/10.1186/s40517-020-00178-5

[19] Heidbach, O., Rajabi, M., Reiter, K., Ziegler, M. (2016) World Stress Map 2016. GFZ Data Services. http://doi.org/10.5880/WSM.2016.002

[20] Gupta, H.K. (2002) A Review of Recent Studies of Triggered Earthquakes by Artificial Water Reservoirs with Special Emphasis on Earthquakes in Koyna, India. *Earth-Science Reviews*, **58**, 279-310. https://doi.org/10.1016/s0012-8252(02)00063-6

[21] Wang, C.Y. and Manga, M. (2021) Water and Earthquakes. Springer. https://doi.org/10.1007/978-3-030-64308-9

[22] Zhao, R., Xue, J. and Deng, K. (2022) Modelling Seismicity Pattern of Reservoir-Induced Earthquakes Including Poroelastic Stressing and Nucleation Effects. *Geophysical Journal International*, **232**, 739-749. https://doi.org/10.1093/gji/ggac361

[23] Smith, P.J. (1982) Reservoirs and the Triggering of Earthquakes. *Nature*, **295**, 9. https://doi.org/10.1038/295009a0

[24] Gupta, H.K. (2018) Review: Reservoir Triggered Seismicity (RTS) at Koyna, India, over the Past 50 Yrs. *Bulletin of the Seismological Society of America*, **108**, 2907-2918. https://doi.org/10.1785/0120180019

[25] Zhang, L., Liao, W., Chen, Z., Li, J., Yao, Y., Tong, G., *et al.* (2022) Variations in Seismic Parameters for the Earthquakes during Loading and Unloading Periods in the Three Gorges Reservoir Area. *Scientific Reports*, **12**, Article No. 11211. https://doi.org/10.1038/s41598-022-15362-9

[26] McGarr, A., Simpson, D. and Seeber, L. (2002) Case Histories of Induced and Triggered Seismicity. *International Geophysics*, **81**, 647-661. https://doi.org/10.1016/s0074-6142(02)80243-1

[27] Foulger, G.R., Wilson, M.P., Gluyas, J.G., Julian, B.R. and Davies, R.J. (2018) Global Review of Human-Induced Earthquakes. *Earth-Science Reviews*, **178**, 438-514. https://doi.org/10.1016/j.earscirev.2017.07.008

[28] Huang, R., Zhu, L., Encarnacion, J., Xu, Y., Tang, C., Luo, S., *et al*. (2018) Seismic and Geologic Evidence of Water-Induced Earthquakes in the Three Gorges Reservoir Region of China. *Geophysical Research Letters*, **45**, 5929-5936. https://doi.org/10.1029/2018gl077639

[29] Guillas, S., Day, S.J. and McGuire, B. (2010) Statistical Analysis of the El Niño-Southern Oscillation and Sea-Floor Seismicity in the Eastern Tropical Pacific. *Philosophical Transactions of the Royal Society A*: *Mathematical*, *Physical and Engineering Sciences*, **368**, 2481-2500. https://doi.org/10.1098/rsta.2010.0044

[30] Martínez-Garzón, P., Beroza, G.C., Bocchini, G.M. and Bohnhoff, M. (2023) Sea Level Changes Affect Seismicity Rates in a Hydrothermal System Near Istanbul. *Geophysical Research Letters*, **50**, e2022GL101258. https://doi.org/10.1029/2022gl101258

[31] Tanaka, S., Ohtake, M. and Sato, H. (2002) Evidence for Tidal Triggering of Earthquakes as Revealed from Statistical Analysis of Global Data. *Journal of Geophysical Research*: *Solid Earth*, **107**, ESE1-1-ESE1-11. https://doi.org/10.1029/2001jb001577